J. Condensed Matter Nucl. Sci. 41 (2026) 153–163

Research Article

Temperature Effects and Transmutations With High Frequency Induction

Heinz B. Winzeler
ecoengineering dr. winzeler, Winterthur-Zurich, Switzerland

Abstract

A compact quartz-glass reactor combining inductive heating and excitation with high magnetic fields was developed to study hydrogen-metal interactions and potential low-energy nuclear phenomena. Experiments with palladium-coated and pure nickel foils produced repeatable activation upon gradual pressure reduction and deactivation by short hydrogen pulses. In the active state, identical output temperatures were maintained with substantially less electrical input, with coefficients of performance ranging from 1.4 to 2.4. Surface analysis by scanning electron microscopy revealed localised melting and pore formation, while energy-dispersive X-ray spectroscopy showed significant compositional changes, including the appearance of elements such as carbon, oxygen, aluminium and silicon. The results demonstrate reproducible excess heat under well-defined conditions and surface changes consistent with nuclear processes, making the reactor a versatile platform for systematic LENR research and scale-up.

Keywords: High-frequency induction, Hydrogen-metal system, Excess heat, Transmutation, Dynamic insulation

1. Introduction

Hydrogen-metal systems have received increasing attention due to their potential to produce clean energy and transmute elements under mild and unconventional conditions [1], [2], [3]. This study presents the results of experiments involving various material configurations. Our experiments are based on the hydrogen-metal gas-phase system discovered by Italian physicists Sergio Focardi and Francesco Piantelli in 1989 [4]. This system was discovered independently in the same year that Fleischmann and Pons observed the electrolysis effect in the USA. Both processes generate nuclear energy without radioactivity. The nuclear nature of the processes was demonstrated by the presence of specific signatures [5]. Piantelli and Focardi's process received little attention at the time. The author considers it to be the more promising of the two.

© 2026 ICCF. All rights reserved. ISSN 2227-3123

2. Reactor Design and Methodology

2.1. Reactor Concept

The reactor is made of quartz glass, allowing both induction heating and optical interaction. It is sealed at the bottom with a flange which allows for the easy exchange of reactants. It contains feedthroughs for sensors and gas at ambient temperature. A central tube that is open to the atmosphere at the bottom contains the temperature sensors. The sensors can be moved freely during the reaction, enabling temperature profiles to be recorded.

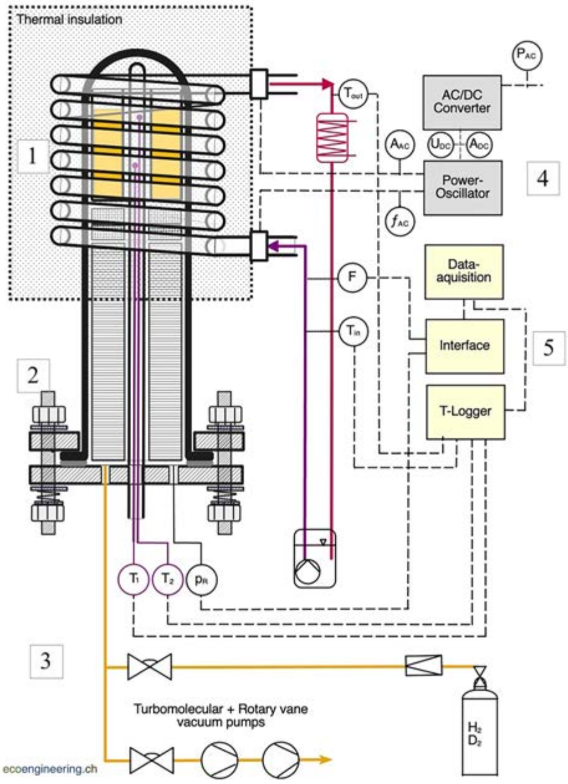

Figure 1. Schematic of the LENR reactor system.

Table 1. Features of the reactor concept.

1.	Hot reaction zone surrounded by a high-frequency induction coil: all energy is coupled inductively (no wiring in the hot zone)
2.	Cold flange with sensor- and gas feedthroughs
3.	Vacuum and gas supply for controlled atmosphere conditioning
4.	Power supply, HF oscillator
5.	Measurement and control system

Fig. 1 shows the P&I diagram of the overall system. Its special features are listed in Table 1. The intellectual property is described in two patents [6] and [7].

A coil is wound around the upper, hot reaction zone. A power oscillator generates an alternating electromagnetic field within the reaction chamber. This heats the reaction material inductively, stimulating interaction between the hydrogen and the metal lattice through the generation of high local currents, all without direct contact.

The induction frequency used was in the range of 102 ± 2 kHz.

Fig. 2 shares the principle of dynamic insulation whose function is described under section 2.3

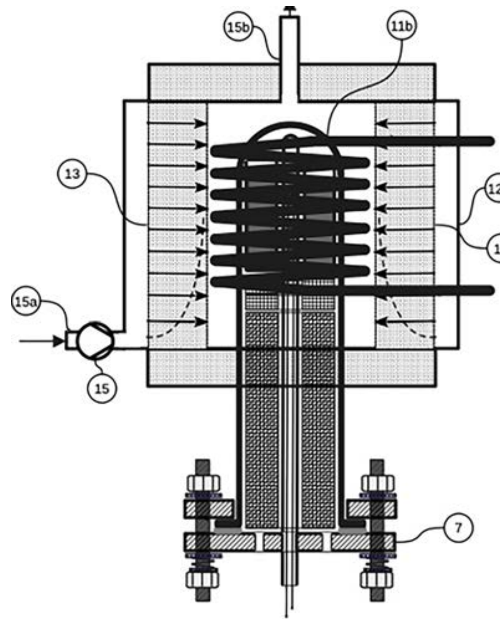

Figure 2. Dynamic insulation.

2.2. Process Equipment, Sensors, Control and Safety Monitoring

Vacuum pumps**:** Rotary vane Alcatel Pascal ACS 2005SD and Turbomolecular Alcatel ATP 80; Flow calibration: Microbalance Mettler Toledo, PM489 DeltaRange 1 mg - 400 g; Valves: Swagelok SS-DS6MM for vacuum and SS-6BRG-MM for hydrogen; 3 piston reciprocating pump for cooling circuit**;** inline filter: Distrelec AG; ZFC75 (04.2023), pressurized gases: H_2 (Linde AG), 10 L, 150 bar, 99.99%; D_2 (Sigma Aldrich), 2 L, 20 bar with pressure reducer 300/1.5 bar (Gloor AG)

Professional components are used for the sensors, pumps and valves. For example: pressure: NXP 100 kPa type MPX2100DP; water flow rate: Digmesa Nano Flowmeter (0.05–0.4 l/min), nozzle (1.1 mm), 49,000 pulses/L, 40 s^{-1}. A 4-channel temperature logger (PCE-T390-4) calibrated and compensated, with an SD card is used with temperature K-type sensors GG-K-30 SLE glass fibre (-30 to 760/1000 °C).

Data acquisition and control: ProfiLab-Expert in combination with a LabJack interface. All the electronics for data acquisition, high-frequency technology, control and safety elements were developed and programmed in-house by team members. Radiation values were continuously measured and recorded using a certified and calibrated device (Gamma-Scout, model Alert) to determine and record any α, β and γ radiation.

2.3. Extraction of Energy - Static and Dynamic Insulation

As shown in Fig. 1, the inductor is designed as a tubular coil through which coolant flows. It acts both as an inducer and a heat exchanger, absorbing and dissipating the heat of the reaction. The hot zone of the reactor is enclosed by static insulation to minimise heat loss.

Fig. 2 shows the reactor equipped with dynamic insulation. The induction coil is made of solid wire and is surrounded by a fluid-permeable insulating material through which a heat transfer fluid (e.g. air) is conducted from the outer containment to the reactor wall. In a counterflow this fluid dissipates the heat emitted by the reactor core and transfers the heat energy to an external recipient with practically no loss.

2.4. Materials and Procedures

2.4.1. *Reaction materials*

Nickel foil rings measuring 20 × 8 × 0.1 mm were electrolytically plated in a bath containing 80 % by weight palladium and 20 wt-% nickel. The resulting thickness of the palladium/nickel layer was 2.6 ± 0.03 μm (Fischerscope X-ray XDV). The total mass of the reaction material was 3.01 g, while the amount of palladium in the reactor was around 205 mg. For surface composition reference is made to section 3.4.2. Plain Ni foils see section 3.5

2.4.2. *Preconditioning*

To remove volatile impurities, a stack of metal rings was pretreated in two stages in the reactor, while the inductor winding was water-cooled: The material was baked under a vacuum of ∼2 Pa for 8 hours using a rotary vane vacuum pump at 200–300 °C. Heating was then continued for a further six hours under a high vacuum of ∼10 mPa using a rotary vane pump and a turbomolecular pump in series. The temperature was gradually increased from 300 to 500 °C.

2.4.3. *Adsorption of hydrogen*

Hydrogen adsorption occurred in cycles of evacuation to 3 mbar and refilling with hydrogen to 0.8 bar. This procedure was repeated four times at 200 °C. The hydrogen loading in the palladium-coated nickel reactant was maintained at temperatures within the range of 190–300 °C and at H_2 pressure typically between 0.5 and 0.8 bar. The H_2 pressure decreased from 0.9 bar to 0.45 bar within 42 hours.

3. Experimental Results

3.1. Temperature Effects

The relationship between temperature, DC input power for induction, and hydrogen pressure was recorded for palladium/nickel-coated nickel foil over a period of approximately 2,000 hours (see Fig. 3).

Three distinct temperature effects appear each with a controlled, slow reduction in H_2 pressure (green curve). This triggers a steady rise in temperature. Significant and repeatable temperature increases are typical of the experiments involving a Ni-Pd stack in a high-frequency field (see the red curves for $\mathrm{T_{R1}}$ and $\mathrm{T_{R2}}$ with K-type sensors 10 mm apart). With a constant electrical input power of either 24 or 30 W, this indicates an exothermic process (see section 3.3). Each increase of temperature ends with a sharp kink, marked with black arrows, before transitioning to a long-lasting constant level. A short H_2 pulse stops the temperature anomaly and returns the reactor temperature to its initial value.

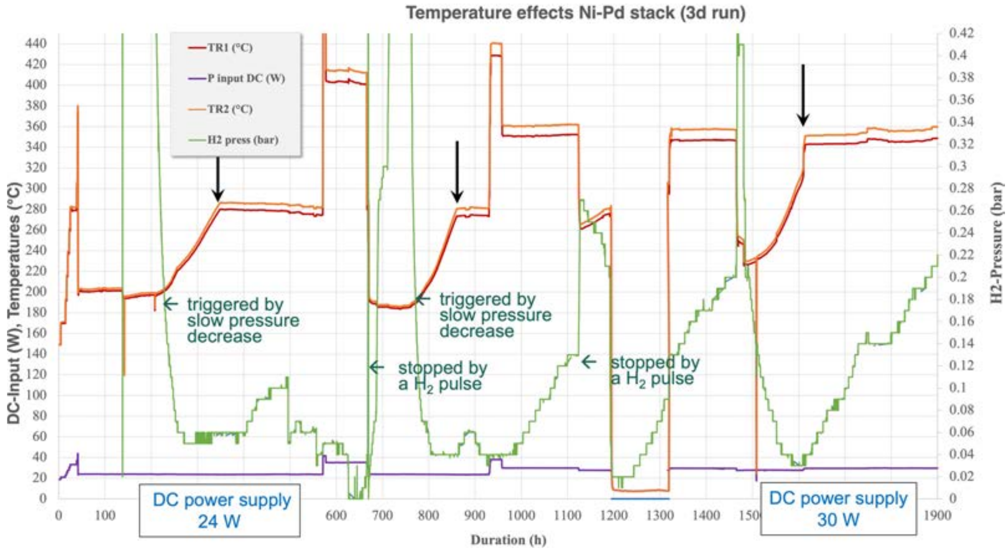

Figure 3. Test procedure over 2000 hours.

Another peculiarity is that once a constant temperature is reached, the gas pressure rises. A sudden leak can be ruled out as the pressure remained constant for around 120 hours and the system underwent repeated vacuum tests. Further clarification is needed to determine whether this could be a reaction product.

3.2. Starting and Stopping the Effect

Reducing the H_2 pressure slowly to below 100 mbar triggers the effect. The temperature increased by 80 K at a constant power input of 24 W DC, rising from 200 to 280 °C and by 120 K at a constant power input of 30 W DC rising from 230 to 350 °C. It takes about 120-150 hours for the temperature to rise to a constant activated state, which is a kind of stable equilibrium. After the distinct kink it remains there for weeks as shown in Fig. 3, for example, from 340 to 500 hours.

After exposing the system to a short H_2 pressure pulse of around 300 mbar, the temperature returns to its initial value within a few minutes.

3.3. Excess Heat

Measurements indicate consistent power gain under specific activation conditions.

Figure 4 shows the results of the step tests, comparing the reactor temperatures before ('inactive) and after activation ('activated) as a function of the power supplied to the inductor. Two example points illustrate the differences between the inactive (orange curve) and active (red curve) states. The temperature of 280 °C is reached at 23 W instead of 33 W and that of 380 °C is reached at 31.5 W instead of 44 W. This indicates that, after activation, the system requires 10–12.5 W less electrical power to reach the same reactor temperature. This equates to a 28% decrease in required electrical heating at 380 °C. Excess heat is generated with a coefficient of performance (COP) of approximately 1.4.

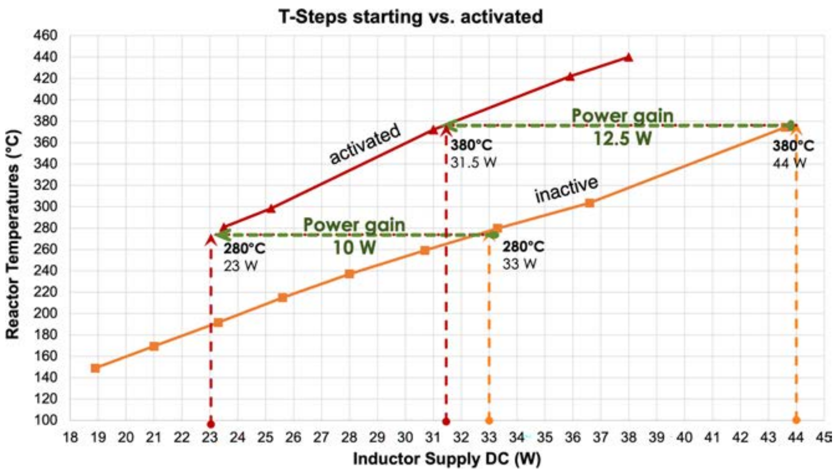

Figure 4. Reactor temperatures as a function of the power supplied to the induction generator.

3.4. Surface Morphology and Composition

Scanning electron microscopy (SEM) and energy-dispersive X-ray analysis (EDX) were used to analyse the palladium-nickel-coated (Ni) foils of the initial material as well as the material that had reacted after thermal treatment under H_2. These analyses were carried out at the Nanoimaging Lab of the Swiss Nanoscience Institute at the University of Basel.

3.4.1. *Surface imaging by scanning electron microscopy (SEM)*

Scanning electron microscopy (SEM) reveals striking changes to the surface, including localised zones of melting and a pattern of scattered holes (Fig. 5 and 6). In a few cases, some of these holes appear to be aligned along crystal boundaries. Since palladium has a melting point of 1550 °C, it is melting and recrystallising locally around these holes at average reactor temperatures of 200 to 500 °C. These zones may be nuclear-active environments.

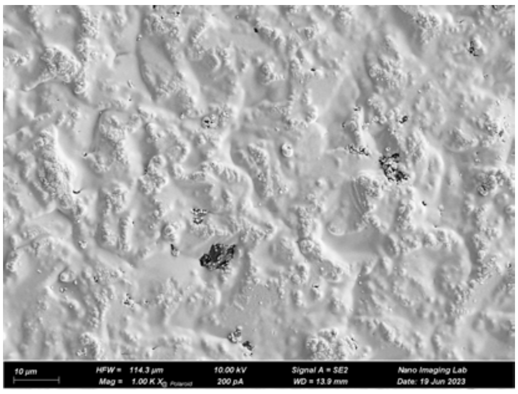

Figure 5. SEM of Pd/Ni coated Ni-foil before.

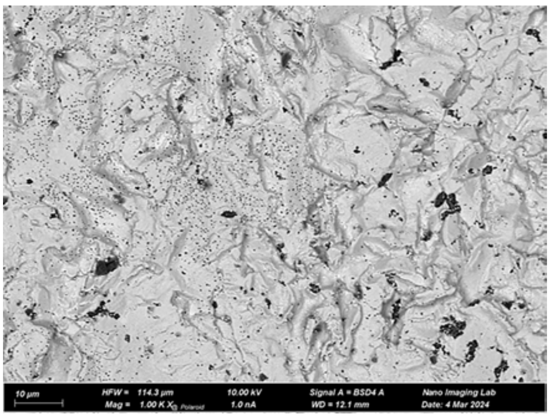

Figure 6. After reaction.

3.4.2. *Surface composition by energy dispersive X-ray analysis (EDX)*

Pre- and post-reaction samples show significant differences in element composition. New elements, such as C, O, Si and Al, were analysed with substantial weight percentages at the surfaces (Fig. 7 and 8).

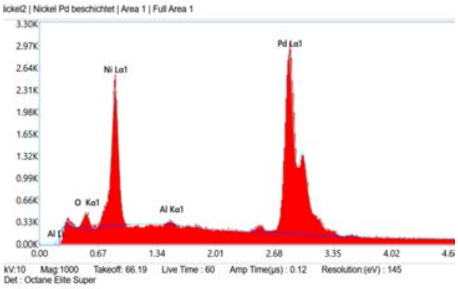

eZAF Quant Result - Analysis Uncertainty: 5.69 %

Element	Weight %	MDL	Atomic %	Error %
O K	3.1	0.55	15.3	14.6
Al K	0.3	0.28	0.8	62.4
Ni L	19.6	1.28	26.5	8.7
Pd L	77.1	0.98	57.5	4.4

Figure 7. EDX Analysis before.

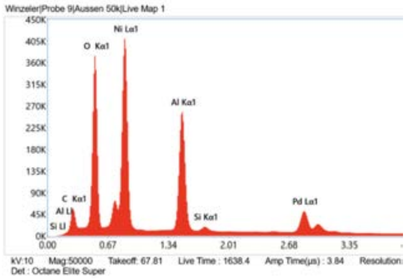

eZAF Quant Result - Analysis Uncertainty: 12.37 %

Element	Weight %	MDL	Atomic %	Error %
C K	8.2	0.09	18.9	9.6
O K	25.9	0.02	44.9	7.5
Al K	14.6	0.02	15.0	4.9
Si K	0.6	0.02	0.6	5.5
Ni L	34.4	0.09	16.3	6.6
Pd L	16.3	0.08	4.3	3.4

Figure 8. After reaction.

In addition to isolated areas that remained inactive, melt zones and perforated surfaces yielded the following analysis values (Table 2):

Table 2. Elements on the surface of the probes after reaction.

EDX	Starting material				Reacted material (at different positions)									
Chemical elements	Starting mat1	Starting Mat.2	Starting Mat.3	**Start average**	inside edge 1kx	insside 5 kx	inside 6	inside 50kx	center	outs edge1 kx	outside n 5kx	bright zone	outside 50 kx	**Reacted average (w-%)**
C	0	0.0	0.0	**0.0**	4.0	8.0	4.0	12.6	3.2	3.2	5.5	**19.0**	8.2	**7.5**
O	4.1	4.3	2.4	**3.6**	9.8	12.6	8.0	16.7	11.9	11.9	18.0	**49.6**	25.9	**18.3**
Al	0.5	0.6	0.0	**0.4**	1.2	3.0	1.3	0.8	1.3	1.3	**11.5**	4.0	14.6	**4.3**
Si					0.9	3.1	0.9	6.1	2.0	2.0	0.8	**16.5**	0.6	**3.7**
Ni	18.5	18.5	20.0	**19.0**	59.5	62.4	59.5	33.9	53.3	53.3	52.5	0.0	34.4	**45.4**
Pd	76.7	76.6	77.6	**77.0**	24.7	10.9	24.7	27.5	28.4	28.4	11.7	8.8	16.3	**20.2**
check sum	99.8	100	100	100	100.1	100	98.4	97.6	100.1	100.1	100	97.9	100	99.4

3.5. Pure Nickel Foils and Hydrogen Gas

In the most recent experiments nickel foil[1] was used with H_2. This was originally intended as a preliminary test for nickel foil with a pure palladium coating. Using 4.47 g of pure nickel foil and a DC input of 109.3 W a temperature of 667 °C was produced. Figure 9 shows a set of step test curves (T, P_{DC} input) in the inactive state at different H_2 pressures for untreated nickel foil. The bottom grey line shows the temperature curve of the reactor system when it

[1] H+S Präzisionsfolien GmbH; Fe = 0.02%; Mg = 0.01%; Co = 0.01%.

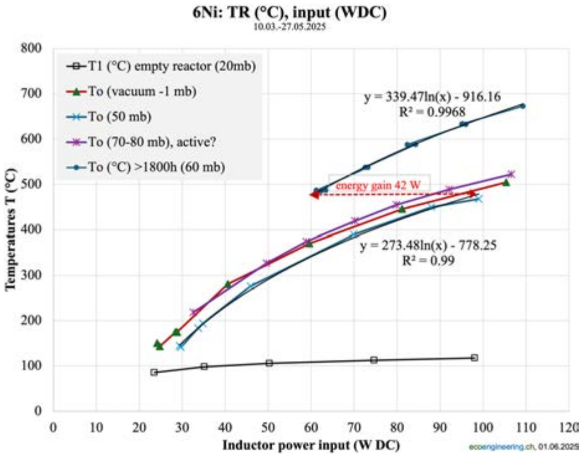

Figure 9. T, input at inactive and active state.

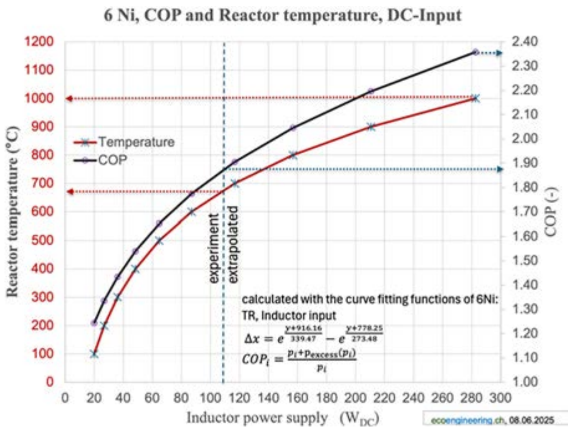

Figure 10. COP with plain Ni and extrapolated.

contains no reacting material, i.e. only the thermocouples. The middle set of curves shows the test of the influence of hydrogen pressure on nickel foil in the inactive state. The top curve shows the temperature behaviour in the active state at 60 mbar.

An input of 109.3 W was found to give a coefficient of performance (COP) of 1.87 $\pm$ 0.1. Curve fitting and extrapolation suggest that an input of approximately 280 W would be required to reach a temperature of around 1000 °C, giving a COP of 2.36 (see Fig. 10).

While temperature measurements are accurate to 1 K and flow measurements have a margin error of 10%, calorimetric measurements only provide rough indications. Considering the somewhat unstable efficiency of the inductor (0.37–0.43) and the fact that the device is still far from optimised, the thermal balance data are consistent with these values.

4. Discussion

The inductively heated and activated reactor consistently produced temperature rises and measurable excess heat under well-defined conditions. Comparable calorimetric signatures have been reported for gas-phase Ni–H systems and metal-hydride composites under dynamic loading conditions [8], [9]. Inductive excitation in the 100 kHz range, as applied here, represents a rarely explored method of activating such systems, enabling both thermal and electromagnetic stimulation without electrical contact to the active core.

4.1. Mechanism of Activation and Deactivation

Activation was reproducibly triggered by a gradual reduction in hydrogen pressure, while deactivation was induced with short H_2 pulses. This behaviour implies a controllable mechanism governed by hydrogen concentration dynamics within the lattice. Cyclic loading may rearrange hydride areas, producing metastable configurations of high local hydrogen density. Kitamura et al. [9] demonstrated that Pd/Ni ratios strongly affect excess power generation, suggesting that the 80:20 w/w Pd–Ni coatings used here may favour optimal hydrogen absorption and lattice strain. The repeatable sharp transition from a steady rise to constant temperature values at different power and temperature levels, observed with different materials, cannot be explained by a transition from ferromagnetic to paramagnetic behaviour, as the Curie temperature is a material constant (360 °C for Ni). This equilibrium phase is possibly linked to hydrogen redistribution or local field-induced electronic changes. As Widom and Larsen postulated, certain transitions could be interpreted as threshold phenomena related to hydrogen loading and local electronic shielding [10]. However, no directly comparable observations or theoretical explanation have been reported to date.

Plasma phenomena could be observed in a recent experiment using a micro camera. But it remains speculative whether this temperature kink could be due to the saturation of a plasma effect.

4.2. Excess Heat and Reproducibility

Step tests demonstrated that identical reactor temperatures required substantially less input power in the activated state, indicating an internal energy contribution. The 28 % reduction in electrical power at 380 °C corresponds to a coefficient of performance (COP) of 1.4 and 2.4 at 1000 °C. These values exceed chemical reaction limits by one to two orders of magnitude: typical metal hydride formation enthalpies are < 0.1 eV per atom [11], whereas the observed heat release corresponds up to 10 eV per reacting atom, consistent with proposed LENR mechanisms. Repetition under various conditions confirmed that the effect is stable and reversible, implying that it is not an artefact of instrumentation or external disturbance. The accuracy and reproducibility of the measurements were verified through multiple repetitions and checks.

4.3. Surface Morphology and Compositional Evidence

Surface analyses provide further evidence of reaction-related processes. Scanning electron microscopy (SEM) revealed localised melting zones and pore formation at bulk temperatures well below the melting point of palladium. This pattern differs slightly from the formation of small craters observed previously, on which carbon was analysed [12]. Ruer provides insights into the formation of such surface effects by means of simulations on cathodes [13]. Such effects suggest highly localised energy release, possibly associated with microscopic reaction centres, so-called nuclear active environments [14].

Energy-dispersive X-ray analysis (EDX) revealed a pronounced depletion of palladium in the reacted layer and the appearance of light elements (C, O, Al, Si) that were not detected in the initial state. These compositional changes are unlikely to arise from incidental contamination: other runs (e.g., with pure nickel foil) performed under comparable vacuum, temperature, and hydrogen-loading conditions did not show any corresponding elemental shifts. The relative magnitudes are similar to those reported by Iwamura et al. [15], who studied hydrogen-loaded, nanostructured, nickel-based, multilayer composites exposed to hydrogen. Such consistent observations across independent laboratories reinforce the interpretation of in-situ element formation.

The observed depletion of palladium, as detected by EDX, is thought to be primarily due to the rearrangement of the Pd layer next to the pores through local melting and resolidification rather than consumption in a reaction.

4.4. Possible Nuclear and Electronic Processes

The magnitude of the heat and the formation of new elements both exceed the scope of chemical reactions. Several nuclear-scale mechanisms could account for the results. Widom and Larsen [10] proposed ultra-low-momentum neutron formation via electron screening on hydride surfaces, which could enable subsequent nuclear transmutation without high-energy emission. NASAs lattice-confinement fusion (LCF) model [16] assumes that hydrogen nuclei, confined in metallic lattices, undergo fusion or fission assisted by local electron density. Both frameworks involve strong coupling between lattice electrons and absorbed hydrogen.

The inductive 100 kHz field used here may further enhance these interactions by generating oscillating currents and transient micro-plasmas that concentrate energy in confined lattice regions. Such field-induced effects are consistent with observations of threshold-like temperature transitions and may represent a distinctive excitation pathway. The Structured Atomic Model (SAM) of Kaal et al. [17] offers a geometric description of atomic rearrangements that could explain local element formation through sub-nuclear reconfiguration within a dense-packed atomic core.

Overall, the convergence of calorimetric, morphological, and compositional evidence supports the hypothesis that hydrogen-metal interactions in dynamically excited lattices may lead to nuclear-scale processes occurring under condensed-matter conditions. The observed reproducibility and controllability distinguish this system from earlier open-cell LENR experiments and point toward an electronically mediated nuclear mechanism driven by combined lattice confinement and inductive excitation.

5. Conclusion

The high-frequency induction reactor developed in this work provides a compact and reproducible platform for studying hydrogen-metal interactions under controllable electromagnetic excitation. Furthermore, the concept is ideal for scaling up. It has a wide range of potential technical applications. Experiments with Ni and Pd–Ni foils demonstrated repeatable activation by gradual hydrogen pressure reduction and deactivation by short pressure pulses. In the active state, identical temperatures required significantly less input power, corresponding to a power gain. The COP of 1.4–2.4 that has been achieved so far is a good starting point for further optimisation.

Surface analyses revealed localised melting and the formation of new elements (C, O, Al, Si) that cannot be attributed to chemical contamination. Together, the thermal, morphological, and compositional results indicate that the observed excess energy originates from hydrogen-induced processes involving nuclear interactions at the lattice level.

Future work should include (i) optimisation of induction frequency and coupling efficiency, (ii) comprehensive isotopic and gas analyses to identify possible reaction products such as helium or neon, and (iii) independent replication under calibrated calorimetry. With continued refinement, inductively activated hydrogen-metal systems could contribute not only to clean, radiation-free energy generation but may also open routes toward controlled low-energy transmutation of materials.

Acknowledgements

Working together as a small team was crucial to our success. During my laboratory experiments, electronics and electrical engineers Lucas Egloff and Enrico Lareida provided invaluable support in developing the electronics and data acquisition system, adapting sensors, and installing safety measures. Without their expertise, this research would not have been possible. The project was originally initiated by mechanical engineer Jack R. Metz, who continues to contribute to it. Thanks also go to the Institute for Materials and Process Engineering at the Zurich University of Applied Sciences (ZHAW), which provided laboratory and process engineering equipment, including high-vacuum pumps and a precision scale. We would also like to thank the Nano Imaging Lab at the Swiss Nanoscience Institute (SNI) at the University of Basel for their invaluable thorough analysis. Finally, I am deeply grateful to my wife Monika, who has endured my experiments at home and my nightly evaluations with tireless patience and attentive feedback.

References

[1] Clean Energy from Hydrogen-Metal Systems | CleanHME | Project | Fact Sheet | H2020, CORDIS | European Commission *https://cordis.europa.eu/project/id/951974*

[2] Breakthrough zero-emissions heat generation with hydrogen-metal systems, Hermes EU Grant ID: 952184 Finland. *https://cordis.europa.eu/project/id/952184*

[3] U.S. Department of Energy Announces $10 Million in Funding to Projects Studying Low-Energy Nuclear Reactions | ARPA-E: *https://arpa-e.energy.gov/news-and-events/news-and-insights/us-department-energy-announces-10-million-funding-projects-studying-low-energy-nuclear-reactions.*

[4] S. Focardi, V. Gabbani, V. Montalbano, Piantelli Francesco, and S. Veronesi, Large excess heat production in Ni-H systems, *Il Nuovo Cimento A*, vol. 111, Nov. 1998.

[5] S. Focardi, V. Gabbani, V. Montalbano, F. Piantelli and S. Veronesi, Evidence of Electromagnetic Radiation from Ni-H Systems, in *Condensed Matter Nuclear Science*, World Scientific NJ, London, 2006, pp. 70–80. doi: 10.1142/9789812774354_0005.

[6] H. B. Winzeler, Vorrichtung und Verfahren Zur Gewinnung Thermischer Energie mit Niedrig Energetischer Kernreaktion, WO2023093990A2, June 01, 2023

[7] H. B. Winzeler, Device and Process for Generating Heat Energy using Low-Energy Nuclear Reaction, *US 2025/0022619 A1*, Dec. 16, 2025

[8] E. Storms, The Science of Low Energy Nuclear Reaction, A Comprehensive Compilation of Evidence and Explanations about Cold Fusion. *World Scientific* NJ, London, Singapore, 2007.

[9] A. Kitamura *et al.*, Excess heat evolution from nanocomposite samples under exposure to hydrogen isotope gases, *International Journal of Hydrogen Energy*, vol. 43, no. 33, pp. 16187–16200, Aug. 2018, doi: 10.1016/j.ijhydene.2018.06.187.

[10] A. Widom and L. Larsen, Ultra low momentum neutron catalyzed nuclear reactions on metallic hydride surfaces, *European Physical Journal C*, vol. 46, pp. 107–111, Apr. 2006, doi: 10.1140/epjc/s2006-02479-8.

[11] A. Züttel, Materials for hydrogen storage, *Materials Today*, vol. 6, no. 9, pp. 24–33, Sept. 2003, doi: 10.1016/S1369-7021(03)00922-2.

[12] H. B. Winzeler et al., Inductively activated LENR reactor: *Internatinal Conference on Condensed Matter Nuclear Science,* ICCF25, Szczecin, Poland, Aug. 2023.

[13] J. Ruer, Simulation of Crater Formation on LENR Cathodes Surfaces, *Journal of Condensed Matter Nuclear Science*, vol. 12, no. 1, Dec. 2013, doi: 10.70923/001c.72226.

[14] Storms, Edmund, An Explanation of Low-energy Nuclear Reactions (Cold Fusion), *J. Condensed Matter Nucl. Sci.*, vol. 9, pp. 1–22, 2012.

[15] Y. Iwamura, T. Itoh, S. Yamauchi, and T. Takahashi, Anomalous heat generation that cannot be explained by known chemical reactions produced by nano-structured multilayer metal composites and hydrogen gas, *Japanese Journal of Applied Physics*, vol. 63, Feb. 2024, doi: 10.35848/1347-4065/ad2622.

[16] T. L. Benyo, Lattice Confinement Fusion (LCF) Overview, Mar. 2023. *https://ntrs.nasa.gov/citations/20230003100*

[17] J. E. Kaal, J. G. Emming, A. Otte, and J. A. Sorensen, *The Nature of the Atom: An Introduction to the Structured Atom Model.* Curtis Press, 2021.